HHS Public Access

Author manuscript

Neuroimage. Author manuscript; available in PMC 2021 January 12.

Published in final edited form as:

Neuroimage. 2020 November 01; 221: 117183. doi:10.1016/j.neuroimage.2020.117183.

Changes in spinal cord hemodynamics reflect modulation of spinal network with different parameters of epidural stimulation

Shanshan Tang[a,1], **Carlos A. Cuellar**[b,c,1], **Pengfei Song**[a], **Riazul Islam**[b], **Chengwu Huang**[a], **Hai Wen**[b], **Bruce E. Knudsen**[b], **Ping Gong**[a], **U-Wai Lok**[a], **Shigao Chen**[a,d,*], **Igor A. Lavrov**[b,d,e,*]

[a]Department of Radiology, Mayo Clinic, Rochester, MN 55905, United States

[b]Department of Neurology, Mayo Clinic, Rochester, MN 55905, United States

[c]Centro de Investigación en Ciencias de la Salud (CICSA), Universidad Anáhuac México Campus Norte, Estado de México, Huixquilucan 52786, México

[d]Department of Physiology and Biomedical Engineering, Mayo Clinic, Rochester, MN 55905, United States

[e]Institute of Fundamental Medicine and Biology, Kazan Federal University, Kazan 420006, Russia

Abstract

In this study functional ultrasound (fUS) imaging has been implemented to explore the local hemodynamics response induced by electrical epidural stimulation and to study real-time *in vivo* functional changes of the spinal cord, taking advantage of the superior spatiotemporal resolution provided by fUS. By quantifying the hemodynamics and electromyographic response features, we tested the hypothesis that the temporal hemodynamics response of the spinal cord to electrical epidural stimulation could reflect modulation of the spinal circuitry and accordingly respond to the changes in parameters of electrical stimulation. The results of this study for the first time demonstrate that the hemodynamics response to electrical stimulation could reflect a neural-vascular coupling of the spinal cord. Response in the dorsal areas to epidural stimulation was

*Corresponding authors. chen.shigao@mayo.edu (S. Chen), lavrov.igor@mayo.edu (I.A. Lavrov).

Author contributions

S.T., C.C., P.S., S.C., R.I., and I.L. designed the experiment. S.T., C.C., P.S., R.I., P.G., U.L., and I.L. drafted the manuscript. S.T., C.C., P.S., R.I., C.H. collected experiment data. S.T. and P.S. wrote the algorithms for data processing. C.C., R.I., H.W., B.E.K. conducted the animal surgeries. All authors reviewed and participated in editing the manuscript.

[1]Co-first authors

Ethics statement

Experiment procedures were approved by the Mayo Clinic Institutional Animal Care and Use Committee. The National Institutes of Health Guidelines for Animal Research (Guide for the Care and Use of Laboratory Animals) were observed rigorously. Animals were kept in controlled environment (21 °C, 45% humidity) on a 12-h light/dark cycle with ad libitum access to water and food.

Data and code availability statement

The original data and processing code script written in MATLAB are available upon request.

Declaration of Competing Interest

The authors declare no competing interests.

Supplementary materials

Supplemental Video 1. Hemodynamics response with sub-threshold intensity.

Supplementary material associated with this article can be found, in the online version, at doi: 10.1016/j.neuroimage.2020.117183.

significantly higher and faster compared to the response in ventral spinal cord. Positive relation between the hemodynamics and the EMG responses was observed at the lower frequencies of epidural stimulation (20 and 40 Hz), which according to our previous findings can facilitate spinal circuitry after spinal cord injury, compared to higher frequencies (200 and 500 Hz). These findings suggest that different mechanisms could be involved in spinal cord hemodynamics changes during different parameters of electrical stimulation and for the first time provide the evidence that neural-vascular coupling of the spinal cord circuitry could be related to specific organization of spinal cord vasculature and hemodynamics.

Keywords

Spinal cord; Hemodynamics responses; Epidural electrical stimulation; Functional ultrasound

1. Introduction

Spinal cord electrical stimulation (SCS) has been implemented earlier to alleviate chronic pain and in the last decade, clinical trials have shown that SCS can restore volitional, motor function in patients suffering spinal cord injury (M. Capogrosso et al., 2013; Kapural, 2014; Young and Stanley, 1979; Agari and Date, 2012; Fénelon et al., 2012; Harkema et al., 2011; Angeli et al., 2014; Harkema et al., 2018; Grahn et al., 2017; Gill et al., 2018). Interestingly, participants on those trials have also experienced improvements in autonomic function, namely cardiovascular, sexual, and voiding. Additionally, reports on other neurological conditions have shown benefits from SCS (Zhong et al., 2019; Santana et al., 2014; Fuentes et al., 2009; Fuentes et al., 2010; Waltz et al., 1981). Regardless the wide application of this technique, there is still limited understanding of the mechanisms of SCS effect on spinal circuitry.

Computational models (M. Capogrosso et al., 2013; Ladenbauer et al., 2010; Rattay et al., 2000) and available in vivo and in vitro electrophysiological assessments (Lavrov et al., 2006; Gerasimenko et al., 2006; Lavrov and Cheng, 2008; Lavrov and Cheng, 2004; Cuellar et al., 2017) have shed some light on the potential components of neural circuits activated by SCS, although, this information is limited and cannot provide deep insight into neurophysiologic mechanisms of SCS effect. This is largely due to the absence of sensitive and reliable tools that could provide critical information about spatial-temporal activation of spinal circuits. For instance, current approaches aim to target the spinal circuitry by using neuromodulation with electrical, magnetic, or pharmacological influence, while using electrophysiological assessment for output measuring i.e. electromyography (EMG). This wide used recording technique provides one dimensional signal reflecting the electrical activity produced by skeletal muscles as a reflection of activation level of neural circuit and although useful, is susceptible to the noise generated by movements during breathing or during muscle contraction caused by electrical stimulation (DeLuca, 2006; Gad et al., 2012).

Functional neuroimaging techniques, such as fMRI, PET, and MEG are successful in mapping neural-vascular coupling of the brain (Logothetis et al., 2001; Hämäläinen et al., 1993; Burns et al., 2007); however, these methods have not yet been very effective in

mapping organization of spinal cord due to challenging location and anatomy of the spinal cord. Recently, functional ultrasound imaging (fUS), a sensitive imaging modality with the use of plane-wave ultrasound illuminations at high frame rate, has achieved valuable spatiotemporal resolution to capture the temporal hemodynamics response (Mace et al., 2011; Mace et al., 2013; Song et al., 2019; Deffieux et al., 2018). As an emerging novel technique, fUS has been successfully employed to investigate the temporal changes in blood volume in the whole brain on animal models with better spatiotemporal resolution compared to the aforementioned functional brain imaging modalities (Mace et al., 2011; Mace et al., 2013).

Previously we reported hemodynamics changes in the spinal cord during SCS in two animal models as monitored by fUS. We also described that fUS offers a better sensitivity in mapping and quantifying hemodynamics in the spinal cord and quantifying the spinal cord activity during subthreshold-to-threshold motor responses produced by SCS compared to electrophysiological assessment (Song et al., 2019). These results suggests that fUS can provide assessment of spinal circuitry at subthreshold level of stimulation, when only low threshold afferents are active, which significantly improves capacity to evaluate the spinal circuitry organization in vivo.

In this study we extend our previous observations and hypothesized that the spinal cord hemodynamics response to SCS reflects a temporal modulation of spinal cord circuitry and, accordingly, responds to the changes in parameters of electrical stimulation. In order to test this hypothesis, we evaluated the spinal cord hemodynamics response to the different frequencies, electrodes configurations, as well as different voltage intensities; and quantified the features of hemodynamics response, such as peak increase in blood volume change, the response rate, and the total amount of blood volume change over the time. With this study, we for the first time provide evidence that neural-vascular coupling of the spinal cord circuitry is related to organization of spinal cord hemodynamics as revealed by implementation of a novel fUS approach.

2. Materials and methods

2.1. Animal preparation procedure

Experiment procedures were approved by the Mayo Clinic Institutional Animal Care and Use Committee. The National Institutes of Health Guidelines for Animal Research (Guide for the Care and Use of Laboratory Animals) were observed rigorously. Animals were kept in controlled environment (21 °C, 45% humidity) on a 12-h light/dark cycle with ad libitum access to water and food.

Eight male Sprague-Dawley rats (325–350 gr) were anesthetized with 1.5%−3% isoflurane. The spinal cord was exposed by removing lamina T13-L2 (corresponding approximately to L2 and S1 segments of the spinal cord). Teflon coated stainless steel wires were placed at T13 and L2 and then sutured on dura. A 0.5 mm notch facing the spinal cord was made on the wires, serving as the stimulating electrode. The spine was fixed to minimize the breathing motion with a custom-made frame composed of a clamp holding the Th12 spinous process and two pieces retracting back muscles on both sides. In addition, the pelvic girdle

was held with two rods secured over the coxal bones. Dorsal skin flaps were attached around the frame to form a pool facilitating transducer positioning. Warm saline solution (1.5 ml) was administered S.C. every 2 h. At the end of experiment, animals were euthanized using pentobarbital (150 mg/kg I.P.).

2.2. Experiment setup

A Verasonics Vantage ultrasound system (Verasonics Inc., Kirkland, WA) and a Verasonic high frequency linear array transducer L22–14v (Verasonics Inc., Kirkland, WA) were used in this study to provide transmission waveforms with 15.625 MHz center frequency and 67% bandwidth. The transducer was placed between the T13 and L2 vertebrae with an ultrasound imaging field of view (FOV) align with the spinal cord and intersect with the central canal, as shown in Fig. 1 (a) and 1(b). The transducer was fixed thoroughly throughout the experiment. Mineral oil was used as acoustic coupling between the spinal cord and ultrasound transducer.

To increase the imaging signal-to-noise-ratio (SNR), ultrafast compounding plane wave imaging sequence was used with five steered plane waves transmitted with each steering angle (−4°, −2°, 0°, 2°, 4°) for three repetitions (Urban et al., 2015). With a pulse repetition frequency (PRF) of 28.6 kHz, it took 525 μs to complete the 15 transmissions. A no operation period of 1475 μs was added to the end of the 15 transmissions, to achieve a post-compounding PRF of 500 Hz. The total data recording time was 120 s with 200 ensembles in each second.

In the rat experiment, the stimulation protocol was set as 30 s baseline measurements, 20 s SCS measurements, and 70 s recovery measurements. Five trials were repeated with the exactly same SCS configurations.

2.3. ESS parameters and electrodes configurations

SCS was delivered on the spinal cord of a rat at vertebrae levels T13 and L2. Different stimulation polarities, including monopolar and bipolar stimulations, were used. Monopolar stimulation was applied with the cathode (−) placed on the T13 spinal cord and anode (+) placed in rat's back muscle. In bipolar stimulation, the anode and cathode electrodes were either placed on T13 and caudal L2 spinal cord segments ($R+C-$, "R " for rostral and "C " for caudal accordingly), or in L2 and T13 spinal cord segments ($R-C+$), respectively. Both low frequency ranges of SCS (20 Hz and 40 Hz) and high frequency SCS (200 Hz and 500 Hz) were used in this study and were chosen based on our previous findings with significant variations of stepping performance with SCS applied with these two frequencies in spinal rats (I. Lavrov et al., 2008; I. Lavrov et al., 2008; I. Lavrov et al., 2015; I. Lavrov et al., 2015; Gad et al., 2013; Shah and Lavrov, 2017). Both sub-threshold intensity and supra-threshold intensity electrical stimulation were tested. Due to the difference in motor threshold across the animals, stimulation voltages were carefully selected based on real-time evaluation of EMG signal and gradual increase and decrease of intensity of SCS. The supra-threshold intensity was determined by increasing the voltage to a maximum level at which stimulation produced a strong contraction, without tremble affecting the fUS imaging. The sub-threshold intensity was determined by decreasing the voltage to a subthreshold level

where EMG signal was undistinguished from noise. A summary for the detailed SCS parameters and electrode configurations can be found in Fig. 1 (c).

2.4. Data processing

After coherent compounding, B-mode ultrasound images were processed with phase correlation based sub-pixel motion registration (Foroosh et al., 2002) and singular-value-decomposition (SVD) based cluttering filtering (Yu and Lovstakken, 2010; Urban et al., 2014) to accumulate one frame of Power Doppler (PD) image in each second k,

$$PD(k) = \frac{1}{N}\sum_{i=1}^{N} I_B^2((k-1)\times N + t_i),\ k = 1, 2, \ldots, 120\ (sec), \tag{1}$$

where I_B is the intensity of a filtered B mode ultrasound image which was acquired at 500 Hz after spatial compounding. In this study, the ensemble number N was 200.

Ultrasound PD signal was measured at each imaging pixel to reflect the local blood volume. The temporal spinal cord hemodynamics response to SCS was evaluated by the spinal cord blood volume change (ΔSCBV), which defines the PD signal intensity variation along with the SCS process in the unit of percentage,

$$\Delta SCBV(k) = \frac{PD_{stim}(k) - \overline{PD_{baseline}}}{\overline{PD_{baseline}}} \times 100\% \tag{2}$$

A ΔSCBV response curve under an SCS configuration was obtained by averaging the ΔSCBV response curve of each pixel inside a selected region of interest (ROI) and averaging all 5 repeated trials under this SCS configuration. The ROIs used in this study include the whole ultrasound FOV, dorsal ROI, ventral ROI, rostral ROI, and caudal ROI. From a ΔSCBV curve, quantitative parameters, including the peak response, ascending slope of the response curve (response rate), and area under the curve (AUC) were measured, as illustrated in Fig. 2 (a). Detailed data processing approach could be found in our previous study (Song et al., 2019).

EMG signals from the tibialis anterior and gastrocnemius hind limb muscles were recorded simultaneously in experiments. The fluctuated zero-line of each EMG signal (Fig. 2 (b)) was first extracted and then subtracted from the EMG signal (Fig. 2 (c)). Then, the root mean square (RMS) of the EMG signal during SCS and the RMS of background activity before SCS were measured and ΔEMG was calculated in the unit of percentage,

$$\Delta EMG(k) = \frac{RMS_{stim}(k) - \overline{RMS_{baseline}}}{\overline{RMS_{baseline}}} \times 100\% \tag{3}$$

where $RMS_{baseline}$ and RMS_{stim} indicates the RMS of the signal during “Stim OFF ” and “Stim ON ” in Fig. 5 (c). ΔEMG was averaged for the 5 repeated trials for each of the four hind limb muscles where EMG signals were recorded from. The largest ΔEMG among the

four was selected to represent the neuromuscular electrophysiological change under the given SCS.

3. Results

3.1. fUS is a sensitive tool in quantifying the subthreshold-to-threshold motor activation response to SCS

During initial testing, we found that fUS offers valuable sensitivity in quantifying the hemodynamics response in the spinal cord during subthreshold SCS, this is even when the amplitude of motor responses are not distinguishable from electrical noise in the EMG recording. A typical hemodynamics response to the sub-threshold SCS intensity is shown in Fig. 3 (a) and Supplemental video 1, where the ultrasound power Doppler (PD) images were color coded with the measured blood volume change, ΔSCBV. The corresponding ΔSCBV curve is shown in Fig. 3 (b), from which an obvious hemodynamics response to the SCS can be observed primary in the dorsal part of the spinal cord. At the same time, no statistically significant changes in the EMG signal were observed due to the sub-threshold intensity of SCS (Fig. 3 (c)).

SCS voltage intensity inducing subthreshold level of motor responses varied across animals and for sub-threshold motor potentials evoked by SCS, the intensity was determined by gradually decreasing the voltage from a readily observable EMG response to a subthreshold level with no obvious EMG signal. Among EMG recordings with sub-threshold SCS, we applied an offline processing, where an EMG signal was considered as “silent EMG ” only when its root mean square (RMS) increase of EMG signal to the baseline, ΔEMG, is lower than 8% (see Supplemental Fig. S1(a)). During experiments we collected 25 tests (a test means data collected from a given animal with a given SCS parameter and electrode configuration) with sub-threshold SCS, among which 8 tests met the criteria and considered as silent EMG. In these 8 tests SCS was applied at sub-threshold level with frequencies of 20 Hz, 40 Hz, and 200 Hz, and also with monopolar electrode configurations, with bipolar R−C + configuration, and with bipolar R + C− configuration. Similarly, a ΔSCBV with a peak response increase greater than 3% was considered reliable in hemodynamics response parameter measurements (see Supplemental Fig. S1(b)–1(c) and Supplemental video 2 and video 3). The peak response of the ΔSCBV curve was measured for the aforementioned 8 tests, where silent EMG signals were observed. Seven tests of the 8 exhibited obvious responses in fUS imaging with a peak response above the preset cutoff, as shown in Fig. 3 (d), suggesting that evaluation of spinal cord hemodynamics with fUS is more sensitive compared to EMG monitoring during SCS.

3.2. Spinal cord hemodynamics response to SCS is spatially dependent

To evaluate the effect of SCS-induced changes in blood volume in different regions of the spinal cord, ΔSCBV response curves and their response parameters were measured in selected spinal cord regions under various SCS configurations. Fig. 4 (a) depicts typical color-coded hemodynamics response images at their peak blood volume increasing induced by SCS with distinct parameters and electrode configurations (test number, n = 4). The dorsal vs ventral regions and rostral vs caudal regions were manually selected by an operator

along the craniocaudally center line and dorsoventrally center line of the spinal cord section in ultrasound FOV. The dorsal vs ventral regions were indicated by the white dashed lines while the rostral vs caudal regions were indicated by the green dashed lines in Fig. 4 (a), respectively. The length of the dorsal/ventral region is 6–7 mm approximately, for the ultrasound FOV is 12.6 mm wide. The depth of the rostral/caudal region is about 1–1.5 mm.

B1. Dorsal vs . Ventral.—Fig. 4 (b) and (c) show the peak response and AUC in the dorsal and ventral regions of the spinal cord, while Fig. 4 (e) and (f) are the corresponding bar plots. Fig. 4 (b)–(h) include monopolar and bipolar electrode configurations. For monopolar configuration, SCS intensity includes sub-threshold and supra-threshold and frequency includes 20 Hz and 40 Hz; For bipolar configuration ($R+C-$ and $R-C+$), SCS intensity includes sub-threshold and supra-threshold and SCS frequency includes 20 Hz, 40 Hz, 200 Hz and 500 Hz (test number, $n = 78$). Each dot on Fig. 4 (b) and (c) represents the dorsal vs ventral hemodynamics responses from the same rat with the same SCS parameter and electrode configuration. Significant differences (paired t-test, $p < 0.001$) were observed in both peak response and AUC between dorsal and ventral spinal cord regions, as illustrated in Fig. 4 (e) and (f). A significant difference in response rate was also observed between dorsal and ventral regions (paired t-test, $p < 0.001$) at almost all tested SCS configurations, as shown in Fig. 4 (d) and (g) (test number, $n = 78$). Overall, the dorsal region of the spinal cord responded with a higher magnitude and a quicker response rate to the SCS compared to the ventral region, independently to the tested stimulation configurations.

B2. Rostral vs . Caudal.—To evaluate the role of electrode configurations in spinal cord hemodynamics response, rostral vs. caudal peak responses of ΔSCBV recorded with monopolar stimulation, bipolar $R+C-$, and bipolar $R-C+$ stimulation were compared (Fig. 4 (h)). Rostral and caudal regions were defined with the middle line perpendicular to the spinal cord FOV, which was between the T13 and L2 vertebrae. Each dot in Fig. 4 (h) represents the rostral versus caudal hemodynamics responses from the same rat with the same SCS parameter and electrode configuration. Different colors represent tests with different electrode configurations (test number, $n = 78$). No significant difference between rostral and caudal region was found for either configuration, indicating that the basic configurations of epidural electrodes have no significant influence on the spatial distribution of spinal cord hemodynamics response. At the same time, we observed that the rostral-caudal response pattern varied from animal to animal. Among the 8 tested rats, 5 showed significantly higher ΔSCBV response in the rostral region compared to the caudal region (paired t-test, $p < 0.001$), while the rest of three rats showed significantly higher ΔSCBV response in caudal region compare to the rostral region ($p < 0.001$), regardless of the electrode configuration (results not shown).

3.3. Spinal cord hemodynamics response is related to 20 and 40 Hz SCS, but not at higher stimulation frequencies

ΔSCBV peak responses with stimulation frequencies of 20 Hz and 40 Hz compared to stimulation frequencies of 200 Hz and 500 Hz were plotted as a function of ΔEMG, as shown in Fig. 5 (a)–(b). Data presented on Fig. 5 were collected from 5 rats with bipolar SCS configuration ($R+C-$ and $R-C+$) and supra-threshold intensity (test number, $n = 14$

and $n = 13$ for Fig. 5 (a) and 5(b) respectively). At low stimulation frequencies (20 and 40 Hz), ΔSCBV was positively correlated to ΔEMG (Fig. 5 (a)), suggesting that at those frequencies, the spinal cord neuronal activity is related to the hemodynamics response. However, no positive relationship was found in either 200 Hz or 500 Hz (Fig. 5 (b)). Fig. 5 (c) shows the response rate between 40 Hz and 200 Hz SCS, chosen based on our previous findings (I. Lavrov et al., 2008; I. Lavrov et al., 2008; I. Lavrov et al., 2015; I. Lavrov et al., 2015; Gad et al., 2013; Shah and Lavrov, 2017). Each data point in Fig. 5 (c)–5(f) represent the response rates measured from the two frequencies, but the same rat and the same electrode configuration. Comparisons of spinal cord hemodynamics response during 40 Hz vs 200 Hz and 40 Hz vs 500 Hz indicate that the spinal cord blood flow increases at 40 Hz stimulation significantly faster than at high frequencies (paired *t*-test, $p < 0.05$) (Fig. 5 (c) and 5(d)).

4. Discussion

The results of this study for the first time show differential hemodynamics responses in dorsal vs. ventral spinal cord during SCS evidenced by fUS. We found specific features related to parameters of stimulation: (1) even at low stimulation intensities (subthreshold to EMG response), SCS induced clear hemodynamics changes in the dorsal, but not ventral spinal cord, even though the EMG output was silent, which may indicate on critical role of the dorsal horn neurons cumulatively processing a greater amount of the sensory information from dorsal roots afferents compared to low threshold muscle afferent activating the motoneurons and premotor interneurons; (2) significantly higher and faster hemodynamics responses in dorsal regions compared to the ventral spinal cord, and (3) significant differences in spinal cord hemodynamics responses at low and high stimulation frequencies, with a positive relation between the hemodynamics and the EMG response observed at lower frequencies (20 Hz and 40 Hz), but not at higher frequencies (200 Hz and 500 Hz). These results support our initial observation that evaluation of spinal cord hemodynamics provides significantly higher sensitivity compared to in vivo electrophysiological assessment, such as EMG monitoring, during SCS.

Motor threshold responses during SCS were determined based on EMG amplitude, which was higher than background level of activity, so results with ΔEMG lower than a given cutoff were considered as silent EMG data (Supplemental Fig. S1(a)). As we demonstrate in this study, SCS facilitated hemodynamics response primary in dorsal regions of spinal cord, regardless of parameters and electrodes configurations, which further support high sensitivity of fUS in evaluation of local changes in the spinal cord during SCS.

The observed hemodynamics changes are likely correlated with spinal cord functional neuroanatomy and particularly with specific organization of vasculature for the dorsal and ventral spinal cord. The ventral part of the spinal cord has predominantly segmental organization, arranged as a string of beads, while the dorsal regions are usually arranged as one solid column, although varying in thickness at different levels (Siclari et al., 2007; Romanes, 1965; Herren and Alexander, 1939). This specific anatomical organization of the spinal cord vasculature and unique distribution of dorsal and ventral spinal arteries, to some extent divides the spinal cord into two functionally different areas of hemodynamics

(Anderson and Willoughby, 1987; Bowen, 1999), which could explain different response in the dorsal vs. ventral parts of spinal cord to SCS. Although, this unique anatomical difference in organization of the spinal cord vasculature has been known for years, the results of this study for the first time show a correlation between hemodynamics and activation of neural circuitry related to sensory processing (dorsal horn) and motor output (ventral horn).

Interestingly, in this study the orientation of electric field adjusted by variations in polarity of stimulating electrodes did not induce significant changes in spinal cord hemodynamics, as shown in Fig. 2 (h), although the rostral-caudal distribution of hemodynamics response was variable between tested animals, which could be due to the two-dimension-sectional nature of fUS FOV, which images one longitudinal cross-section of the spinal cord, considering the 3 mm spinal cord diameter is thicker than the elevational resolution of the high-frequency transducer used in the study.

5. fUS compared to other imaging techniques to study neural activation in the spinal cord

Hemodynamic responses evoked by peripheral noxious stimulation can be detected using contrast agents during BOLD and BV-weighted fMRI techniques in rats. As expected, dorsal horn activation in lumbar segments at L4 was evidenced although location of activation, surface vs. deeper laminae (V-VI) was varied depending on the fMRI technique (Zhao et al., 2008). At the same time, fMRI signals were not found with non-noxious stimulation (range of 3–70 Hz), either due to limitations of the fMRI techniques, anesthetic effect (α-chloralose) or other factors (Zhao et al., 2008). In our study, we found a clear hemodynamic response in the dorsal area of the spinal cord that was correlated with stimulation frequencies of 20 and 40 Hz, but not higher frequencies (Fig. 5). The hemodynamic response was also evident even at sub-threshold stimulation intensities monitored by EMG (Fig. 3). Discrepancies in terms of absence of detected signals with non-noxious stimulation protocols on fMRI and our findings can be explained in terms of central vs. peripheral stimulation, for instance, during SCS, electrical current readily spreads over the dorsal roots bilaterally (M. Capogrosso et al., 2013) and if delivered in a proper stimulation frequency and intensity, motor activation resembling stepping can be evoked in spinal (Lavrov et al., 2006; Gerasimenko et al., 2003; I. Lavrov et al., 2008) and non-injured awake animals (Gerasimenko et al., 2006), by activation of the spinal locomotor circuitry.

In the study by Brieu et al. (Brieu et al., 2010), peripheral stimulation at the sciatic nerve was delivered and Intrinsic optical imaging (IOI) combined with laser speckle was obtained focusing on the dorsal horn. Hemodynamic responses were observed ipsilaterally with some activation on the contralateral side at higher stimulation intensities peaking around 2 s and reaching a baseline state in a 7–12 s range (Brieu et al., 2010). Our previous results (Song et al., 2019) showed a considerably larger recovery time (baseline) >25 s depending on the stimulation intensity and region of the spinal cord (dorsal, vs. ventral; rostral vs. caudal) that can be also noted on Fig. 3. Differences may arise on electrical stimulation parameters as in the study by Brieu et al. (Brieu et al., 2010) electrical stimulation consisted of a train o 10

pulses (10 ms each) delivered every 19 s, while in our study stimulation lasted 20 s. Additionally, differences in central vs. peripheral stimulation may also account. Urban et al., (Urban et al., 2014) showed that even a single electrical pulse (250 μs) delivered in the forepaw was able to elicit a contralateral response in the somatosensory cortex in rats. In line with our results, fUS showed high sensitivity, detecting an increase in the cerebral blood volume (CVB) of ≈ 3% with a single electrical pulse.

The results of this study suggest that fUS has relatively high spatial and temporal resolution in monitoring the localized hemodynamics response at different spinal cord segments (Song et al., 2019). Although other functional imaging modalities, such as PET and fMRI, have their distinct advantages, such as high sensitivity and excellent imaging contrast and imaging depth, their spatial and/or temporal resolution are far below what is required for evaluation of the spinal cord functional changes, particularly during neuromodulation with SCS. For instance, the imaging FOV of the presented fUS images was 9.9 mm × 12.8 mm with a spatial resolution of 98.56 μm (the wavelength of ultrasound pulses, as well as the pixel size of fUS image) and a temporal resolution of 500 Hz. In contrast, typical spatial resolution of fMRI is 1.5 mm – 3 mm. fMRI with a 7 Tesla machine reaches a spatial resolution of 750 μm by sacrificing the tSNR and detecting sensitivity (Huber et al., 2018; Kemper et al., 2018). In addition, the size of MR or PET machine is a critical limitation for an intraoperative monitoring. Although functional neuroimaging techniques including EEG and MEG have very high temporal resolution, because of interference with electrical field, they could not be applied to study the stimulation related hemodynamics response, where fUS is able to complement.

Factors such as temperature change, autonomic regulation, strenuous activities, etc., may also induce changes in spinal cord blood flow, which can be detected by fUS. Our previous study (Song et al., 2019) demonstrated that during background fUS recording of the spinal cord without electrical stimulation no increase of blood flow signal was observed across multiple tests.

6. Frequency dependent hemodynamics in response to SCS

The results of this study for the first time emphasize a coupling between the spinal cord hemodynamics and spinal circuits activated by SCS at low frequencies (20 Hz – 40 Hz) compared to high frequencies (200 Hz – 500 Hz) and support the hypothesis that different settings of SCS may activate different mechanisms and/or different components of the spinal circuitry. Similar results were presented earlier (Nielsen and Lauritzen, 2001) where the cerebral blood flow in rat somatosensory cortex was found to be highly correlated to the field potentials of electrical stimulation on the infraorbital nerve at low frequencies (< 2 Hz) and uncoupling at stimulation frequencies of 2 – 5 Hz. Although the frequency range in both studies is different that could be due to the different parts of the nervous system and different neural organization.

A coupling between the spinal cord hemodynamics and the neuronal activity facilitated at frequency range 20 Hz – 40 Hz is supported by our early findings where facilitation of the spinal circuitry to maintain optimal stepping pattern was successfully achieved with epidural

stimulation at the similar frequency range (I. Lavrov et al., 2008; I. Lavrov et al., 2008; I. Lavrov et al., 2015; I. Lavrov et al., 2015; Gad et al., 2013; Shah and Lavrov, 2017; Gerasimenko et al., 2001). Although current results may not be sufficient to draw a certain conclusion regarding how particular frequency modulates the spinal cord circuitry, the mechanisms responsible for this effect can be evaluated in future studies by selective stimulation of spinal structures and peripheral nerves or by comparing the effect of SCS with pharmacological activation or inhibition of the different components of spinal network.

7. Limitations of fUS

One of the obstacles to clinical translation of fUS in spinal cord imaging and evaluation is the motion artifacts caused by physiological activities, which may require sophisticated stabilization of the vertebral column and mechanical isolation from the muscles. One caveat to clinical translation of fUS is the direct placement of fUS transducer on the spinal cord with the vertebra removed. However, compared with other functional imaging techniques, such as fMRI and PET, currently fUS has the potential to be applied to freely moving animals with the miniaturized transducers (Urban et al., 2015; Sieu et al., 2015) evaluating functional changes in spinal cord in real time. This limitation of removing vertebra could be potentially solved by miniaturization of the device and the development of implantable ultrasound transducers. In addition, non-invasive fUS with microbubble-enhanced PD technique has been reported (Deffieux et al., 2018; Errico et al., 2016), where fUS can be performed on rats with intact skull. This microbubble-enhanced and non-invasive fUS technique could be adopted for spinal cord imaging in the future.

It should be noted that implementation of fUS for imaging and monitoring of spinal cord reported in this work and in our previously published article (Song et al., 2019) are the first explorations of applying fUS to study spinal cord hemodynamics during epidural stimulation. Although some correlation between spinal cord hemodynamics and activation of neural circuitry is likely related to sensory processing and motor output, more experiments and deeper investigation are needed to establish a valid correlation. Since this work was performed on intact spinal cord, future studies on effect of spinal cord stimulation applied after different severities of spinal cord injury will help to gain critical information on effect of spinal cord stimulation on local hemodynamics after SCI. For instance, animal models of spinal cord injury inflict trauma ranging from mild to severe by using several techniques, affecting not only nervous tissue but vascular as well. fUS could be used to monitor hemodynamics around the site of injury and evaluate early and chronic interventions, for example SCS.

8. Future directions

The results of this study also support a great potential of fUS as a research tools to study spinal cord and as a potential diagnostic tool with several critical clinical applications.

Evaluation of spinal hemodynamics changes may help in optimizing electrodes location and expanding our understanding of the mechanisms of spinal cord neuromodulation and spinal cord functional organization, for example, evaluating of local spinal hemodynamics after

spinal cord injury and during SCS with different stimulation parameters and electrode configurations (Alam et al., 2015). Recently studies demonstrated that rostral lumbar segments are important to provide rhythmicity during steeping in adult rats, compared to caudal segments (Gerasimenko et al., 2019). fUS technique could provide insights into differences in hemodynamic response at rostral vs. caudal lumbar-sacral segments during stepping, i.e. fictive locomotion induced by pharmacological agents or by stimulation of the midbrain or spinal cord. Moreover, SCS has also gained attention as potential treatment for autonomic dysfunction after SCI (Herrity et al., 2018). In this context, fUS could be implemented to study hemodynamics related to the neural circuits involved into regulation of autonomic functions and particularly in regulation of the blood pressure, bladder, and bowel function (Gad et al., 2014; Guiho et al., 2018).

Spinal cord fUS could also help in evaluation of hemodynamics response during electrode implantation to optimize leads location for neuromodulation therapies and for intraoperative monitoring, which cannot be achieved by other functional imaging modality, such as fMRI or PET. fUS may also help to reveal important information about spinal cord circuitry activated during pharmacological interventions and different modalities of neuromodulation to tune dosage or stimulation parameters for more specific delivery of these therapies. The findings that subthreshold epidural stimulation can selectively increase hemodynamics in the dorsal areas of the spinal cord could also lead to development of novel combined pharmacological and neuromodulation treatments, where local pharmacological effect could be further enhanced by activation of local hemodynamics in target area. Spinal cord fUS can be also utilized to investigate the mechanism of pain development and effect of spinal cord neuromodulation, by characterizing associated neurovascular coupling (Dickenson and D'Mello, 2008; Malisza and Stroman, 2002; Jeon, 2012). Other potential applications could include evaluation of spinal cord ischemia and revascularization following SCI, local tumor growth, and others (Seidel and Meairs, 2009; Deng et al., 2016).

9. Conclusions

In summary, results of this study indicate that (1) the dorsal regions of the spinal cord have significantly higher and faster blood volume changes compared to ventral spinal cord region during SCS, regardless of parameters and electrodes configurations; (2) spinal cord hemodynamics changes are more responsive to the low frequencies (20–40 Hz) of stimulation, at which ΔEMG and ΔSCBV were positively related, that was not observed at higher SCS frequencies (200–500 Hz), suggesting the frequency-dependent mechanism of spinal cord hemodynamics response; (3) hemodynamics changes recorded with fUS provide more sensitive approach for evaluation of the spinal cord response to neuromodulation compare to currently available in vivo electrophysiological techniques. This study for the first time explores the role of spinal cord hemodynamics in effect of SCS and suggests that neural-vascular coupling of spinal hemodynamics could be related to spinal neural circuitry. These findings support future development of neuromodulation techniques where the stimulation parameters, electrodes location, and the orientation of the electric field could be precisely tuned based on real-time evaluation of the local changes in spinal cord hemodynamic. Although the mechanisms of presented here findings need further investigations, spinal cord fUS opens a new direction for quantitative evaluation of spinal

cord hemodynamics and understanding the spinal cord neural-vascular coupling and the mechanisms of spinal cord neuromodulation.

Supplementary Material

Refer to Web version on PubMed Central for supplementary material.

Acknowledgment

Research reported in this publication was supported in part by the Minnesota State Office for Higher Education Spinal Cord Injury and Traumatic Brain Injury Research Grant Program (FP00098975 and FP00093993), by the subsidy allocated to Kazan Federal University for the state assignment in the sphere of scientific activities (No. 0671-2020-0059) and the Russian Government Program of Competitive Growth of Kazan Federal University, and the National Cancer Institute (NCI) of the National Institutes of Health (NIH) under Award Number R00CA214523. The content is solely the responsibility of the authors and does not necessarily represent the official views of the National Institutes of Health.

References

Agari T, Date I, 2012 Spinal cord stimulation for the treatment of abnormal posture and gait disorder in patients with Parkinson’s disease. Neurol. Med. Chir. (Tokyo) 52 (7), 470–474. [PubMed: 22850494]

Alam M, et al., 2015 Evaluation of optimal electrode configurations for epidural spinal cord stimulation in cervical spinal cord injured rats. J. Neurosci. Methods 247, 50–57. [PubMed: 25791014]

Anderson NE, Willoughby EW, 1987 Infarction of the conus medullaris. Ann. Neurol 21 (5), 470–474. [PubMed: 3592640]

Angeli CA, et al., 2014 Altering spinal cord excitability enables voluntary movements after chronic complete paralysis in humans. Brain 137 (5), 1394–1409. [PubMed: 24713270]

Bowen BC, 1999 MR angiography of spinal vascular disease: what about normal vessels? Am. J. Neuroradiol 20 (10), 1773–1774. [PubMed: 10588094]

Brieu N, et al., 2010 Characterization of the hemodynamic response in the rat lumbar spinal cord using intrinsic optical imaging and laser speckle. J. Neurosci. Methods 191, 151–157. [PubMed: 20600322]

Burns HD, et al., 2007 MK-9470, a positron emission tomography (PET) tracer for in vivo human PET brain imaging of the cannabinoid-1 receptor. Proceed. Natl. Acad. Sci 104 (23), 9800–9805.

Capogrosso M, et al., 2013a A computational model for epidural electrical stimulation of spinal sensorimotor circuits. J. Neurosci 33 (49), 19326–19340. [PubMed: 24305828]

Capogrosso M, et al., 2013b A computational model for epidural electrical stimulation of spinal sensorimotor circuits. J. Neurosci 33 (49), 19326–19340. [PubMed: 24305828]

Cuellar CA, et al., 2017 The role of functional neuroanatomy of the lumbar spinal cord in effect of epidural stimulation. Front. Neuroanat 11, 82. [PubMed: 29075183]

Deffieux T, et al., 2018 Functional ultrasound neuroimaging: a review of the preclinical and clinical state of the art. Curr. Opin. Neurobiol 50, 128–135. [PubMed: 29477979]

Deng L, et al., 2016 A multi-frequency sparse hemispherical ultrasound phased array for microbubble-mediated transcranial therapy and simultaneous cavitation mapping. Phys. Med. Biol 61 (24), 8476–8501. [PubMed: 27845920]

Dickenson AH, D’Mello R, 2008 Spinal cord mechanisms of pain. BJA: Br. J. Anaesth 101 (1), 8–16. [PubMed: 18417503]

DeLuca CJ, 2006 Electromyography In: Webster JG (Ed.). Encyclopedia of Medical Devices and Instrumentation. John Wiley.

Errico C, et al., 2016 Transcranial functional ultrasound imaging of the brain using microbubble-enhanced ultrasensitive Doppler. Neuroimage 124, 752–761. [PubMed: 26416649]

Fénelon G, et al., 2012 Spinal cord stimulation for chronic pain improved motor function in a patient with Parkinson's disease. Parkinsonism Relat. Disord 18 (2), 213–214. [PubMed: 21865071]

Foroosh H, Zerubia JB, Berthod M, 2002 Extension of phase correlation to subpixel registration. IEEE Trans. Image Process 11 (3), 188–200. [PubMed: 18244623]

Fuentes R, et al., 2009 Spinal cord stimulation restores locomotion in animal models of Parkinson's disease. Science 323, 1578–1582. [PubMed: 19299613]

Fuentes R, et al., 2010 Restoration of locomotive function in Parkinson's disease by spinal cord stimulation: mechanistic approach. Eur. J. Neurosci 32, 1100–1108. [PubMed: 21039949]

Gad P, et al., 2012 Forelimb EMG-based trigger to control an electronic spinal bridge to enable hindlimb stepping after a complete spinal cord lesion in rats. J. Neuroeng. Rehabil 9 (1), 38. [PubMed: 22691460]

Gad P, et al., 2013 Neuromodulation of motor-evoked potentials during stepping in spinal rats. J. Neurophysiol 110 (6), 1311–1322. [PubMed: 23761695]

Gad PN, et al., 2014 Initiation of bladder voiding with epidural stimulation in paralyzed, step trained rats. PLoS ONE 9 (9), e108184. [PubMed: 25264607]

Gerasimenko YP, et al., 2006 Spinal cord reflexes induced by epidural spinal cord stimulation in normal awake rats. J. Neurosci. Methods 157 (2), 253–263. [PubMed: 16764937]

Gerasimenko YP, et al., 2003 Initiation of locomotor activity in spinal cats by epidural stimulation of the spinal cord. Neurosci. Behav. Physiol 33 (3), 247–254. [PubMed: 12762591]

Gerasimenko I, et al., 2001 Initiation of locomotor activity in spinalized cats by epidural stimulation of the spinal cord. Ross. Fiziol. Zh. Im. I.M. Sechenova 87 (9), 1161–1170. [PubMed: 11763528]

Gerasimenko Y, et al., 2019 Rostral lumbar segments are the key controllers of hindlimb locomotor rhythmicity in the adult spinal rat. J. Neurophysiol 122 (2), 585–600. [PubMed: 30943092]

Gill ML, et al., 2018 Neuromodulation of lumbosacral spinal networks enables independent stepping after complete paraplegia. Nat. Med 24 (11), 1677–1682. [PubMed: 30250140]

Grahn PJ, et al., 2017 Enabling task-specific volitional motor functions via spinal cord neuromodulation in a human with Paraplegia. Mayo Clin. Proc 92, 544–554. [PubMed: 28385196]

Guiho T, et al., 2018 Impact of direct epispinal stimulation on bladder and bowel functions in pigs: a feasibility study. Neurourol. Urodyn 37 (1), 138–147. [PubMed: 28605134]

Hämäläinen M, et al., 1993 Magnetoencephalography-theory, instrumentation, and applications to noninvasive studies of the working human brain. Rev. Mod. Phys 65 (2), 413–497.

Harkema S, et al., 2011 Effect of epidural stimulation of the lumbosacral spinal cord on voluntary movement, standing, and assisted stepping after motor complete paraplegia: a case study. Lancet 377 (9781), 1938–1947. [PubMed: 21601270]

Harkema SJ, et al., 2018 Normalization of blood pressure with spinal cord epidural stimulation after severe spinal cord injury. Front. Hum. Neurosci 12 (83).

Herren R, Alexander L, 1939 Sulcal and intrinsic blood vessels of human spinal cord. Arch. Neurol. Psychiatry 41 (4), 678–687.

Herrity AN, et al., 2018 Lumbosacral spinal cord epidural stimulation improves voiding function after human spinal cord injury. Sci. Rep 8 (1), 8688. [PubMed: 29875362]

Huber L, Ivanov D, Handwerker DA, Marrett S, Guidi M, Uludag K, et al., 2018 Techniques for blood volume fMRI with VASO: from lowresolution mapping towards sub-millimeter layer-dependent applications. Neuroimage 164, 131–143. [PubMed: 27867088]

Jeon YH, 2012 Spinal cord stimulation in pain management: a review. Korean J. Pain 25 (3), 143–150. [PubMed: 22787543]

Kapural L, 2014 Spinal cord stimulation for intractable chronic pain. Curr. Pain Headache Rep 18 (4), 406. [PubMed: 24595705]

Kemper VG, De Martino F, Emmerling TC, Yacoub E, Goebel R, 2018 High resolution data analysis strategies for mesoscale human functional MRI at 7 and 9.4T. Neuroimage 164, 48–58. [PubMed: 28416453]

Ladenbauer J, et al., 2010 Stimulation of the human lumbar spinal cord with implanted and surface electrodes: a computer simulation study. IEEE Trans. Neural Syst. Rehabil. Eng 18 (6), 637–645. [PubMed: 21138794]

Lavrov I, et al., 2006 Plasticity of spinal cord reflexes after a complete transection in adult rats: relationship to stepping ability. J. Neurophysiol 96 (4), 1699–1710. [PubMed: 16823028]

Lavrov I, Cheng J, 2008 Methodological optimization of applying neuroactive agents for the study of locomotor-like activity in the mudpuppies (Necturus maculatus). J. Neurosci. Methods 174 (1), 97–102. [PubMed: 18692523]

Lavrov I, Cheng J, 2004 Activation of NMDA receptors is required for the initiation and maintenance of walking-like activity in the mudpuppy (Necturus Maculatus). Can. J. Physiol. Pharmacol 82 (8–9), 637–644. [PubMed: 15523521]

Lavrov I, et al., 2008a Facilitation of stepping with epidural stimulation in spinal rats: role of sensory input. J. Neurosci 28 (31), 7774–7780. [PubMed: 18667609]

Lavrov I, et al., 2008b Epidural stimulation induced modulation of spinal locomotor networks in adult spinal rats. J. Neurosci 28 (23), 6022–6029. [PubMed: 18524907]

Lavrov I, et al., 2015a Integrating multiple sensory systems to modulate neural networks controlling posture. J. Neurophysiol 114 (6), 3306–3314. [PubMed: 26445868]

Lavrov I, et al., 2015b Activation of spinal locomotor circuits in the decerebrated cat by spinal epidural and/or intraspinal electrical stimulation. Brain Res. 1600, 84–92. [PubMed: 25446455]

Lavrov I, et al., 2008c Epidural stimulation induced modulation of spinal locomotor networks in adult spinal rats. J. Neurosci 28 (23), 6022–6029. [PubMed: 18524907]

Logothetis NK, et al., 2001 Neurophysiological investigation of the basis of the fMRI signal. Nature 412, 150. [PubMed: 11449264]

Mace E, et al., 2011 Functional ultrasound imaging of the brain. Nat. Methods 8 (8), 662–664. [PubMed: 21725300]

Mace E, et al., 2013 Functional ultrasound imaging of the brain: theory and basic principles. IEEE Trans. Ultrason. Ferroelectr. Freq. Control 60 (3), 492–506. [PubMed: 23475916]

Malisza KL, Stroman PW, 2002 Functional imaging of the rat cervical spinal cord. J. Magn. Reson. Imaging 16 (5), 553–558. [PubMed: 12412032]

Nielsen AN, Lauritzen M, 2001 Coupling and uncoupling of activity-dependent increases of neuronal activity and blood flow in rat somatosensory cortex. J. Physiol. (Lond.) 533 (3), 773–785. [PubMed: 11410634]

Rattay F, Minassian K, Dimitrijevic MR, 2000 Epidural electrical stimulation of posterior structures of the human lumbosacral cord: 2. quantitative analysis by computer modeling. Spinal Cord 38, 473. [PubMed: 10962608]

Romanes GJ, 1965 The arterial blood supply of the human spinal cord. Paraplegia 2, 199. [PubMed: 14261502]

Santana MB, et al., 2014 Spinal cord stimulation alleviates motor deficits in a primate model of Parkinson disease. Neuron. 84 (4), 716–722. [PubMed: 25447740]

Seidel G, Meairs S, 2009 Ultrasound contrast agents in ischemic stroke. Cerebrovasc. Dis 27 (suppl 2), 25–39 (Suppl. 2).

Shah PK, Lavrov I, 2017 Spinal epidural stimulation strategies: clinical implications of locomotor studies in spinal rats. Neuroscientist 23 (6), 664–680. [PubMed: 28345483]

Siclari F, et al., 2007 Developmental anatomy of the distal vertebral artery in relationship to variants of the posterior and lateral spinal arterial systems. AJNR Am. J. Neuroradiol 28 (6), 1185–1190. [PubMed: 17569985]

Sieu LA, et al., 2015 EEG and functional ultrasound imaging in mobile rats. Nat Methods 12, 831–834. [PubMed: 26237228]

Song P, et al., 2019 Functional ultrasound imaging of spinal cord hemodynamic responses to epidural electrical stimulation: a feasibility study. Front. Neurol 10, 1–13. [PubMed: 30761061]

Urban A, et al., 2014 Chronic assessment of cerebral hemodynamics during rat forepaw electrical stimulation using functional ultrasound imaging. NeuroImage, 2014 101, 138–149.

Urban A, et al., 2015 Real-time imaging of brain activity in freely moving rats using functional ultrasound. Nat. Methods 12, 873. [PubMed: 26192084]

Waltz JM, et al., 1981 Multi-lead spinal cord stimulation for control of motor disorders. Appl. Neurophysiol 44, 244–257. [PubMed: 6978682]

Young RF, Stanley SJ, 1979 Dorsal spinal cord stimulation in the treatment of multiple sclerosis. Neurosurgery 5 (2), 225–230. [PubMed: 314606]

Yu ACH, Lovstakken L, 2010 Eigen-based clutter filter design for ultrasound color flow imaging: a review. IEEE Trans. Ultrason. Ferroelectr. Freq. Control 57 (5), 1096–1111. [PubMed: 20442020]

Zhao F, et al., 2008 BOLD and blood volume-weighted fMRI of rat lumbar spinal cord during non-noxious and noxious electrical hindpaw stimulation. Neuroimage 40 (1), 133–147. [PubMed: 18164630]

Zhong H, et al., 2019 Epidural spinal cord stimulation improves motor function in rats with chemically induced Parkinsonism. Neurorehabil. Neural Repair 33 (12), 1029–1039. [PubMed: 31684831]

Significance statement

Spinal cord electrical epidural stimulation (SCS) has been successfully applied to control chronic refractory pain and was evolved to alleviate motor impairment after spinal cord injury, in Parkinson's disease, and other neurological conditions. The mechanisms underlying the SCS remain unclear, and current methods for monitoring SCS are limited in sensitivity and spatiotemporal resolutions to evaluate functional changes in response to SCS. We tested the hypothesis that the temporal hemodynamics response of the spinal cord to SCS could reflect modulation of the spinal cord circuitry and accordingly respond to the changes in parameters of SCS. The proposed methodology opens a new direction for quantitative evaluation of the spinal cord hemodynamics in understanding the mechanisms of spinal cord neural-vascular coupling and effect of neuromodulation.

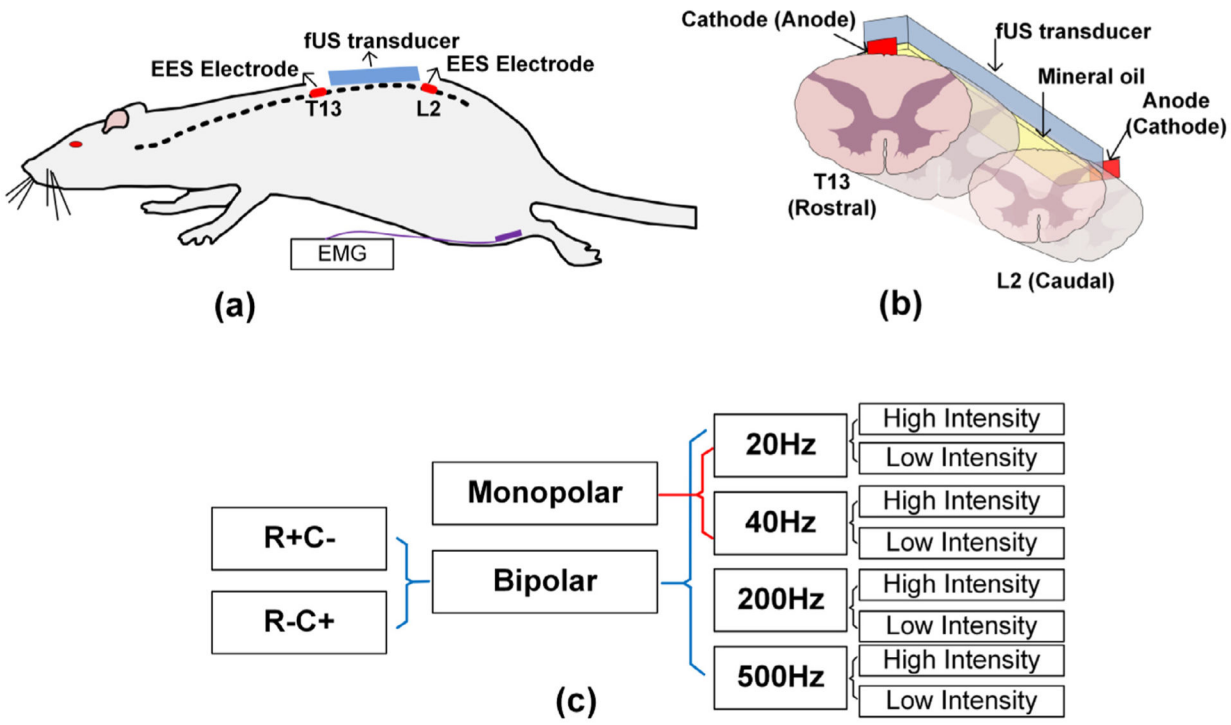

Fig. 1.

Experiment setup and SCS parameters and electrode configurations. (a) and (b) illustrates the positioning of ultrasound transducer, spinal cord electrodes, and the EMG electrodes. (c) Detailed SCS configurations. $R+$ $C-$ represents the anode is placed at spinal cord T13 while the cathode is placed at spinal cord L2. R$-$ $C+$ represents the opposite placement (R for rostral and C for caudal accordingly).

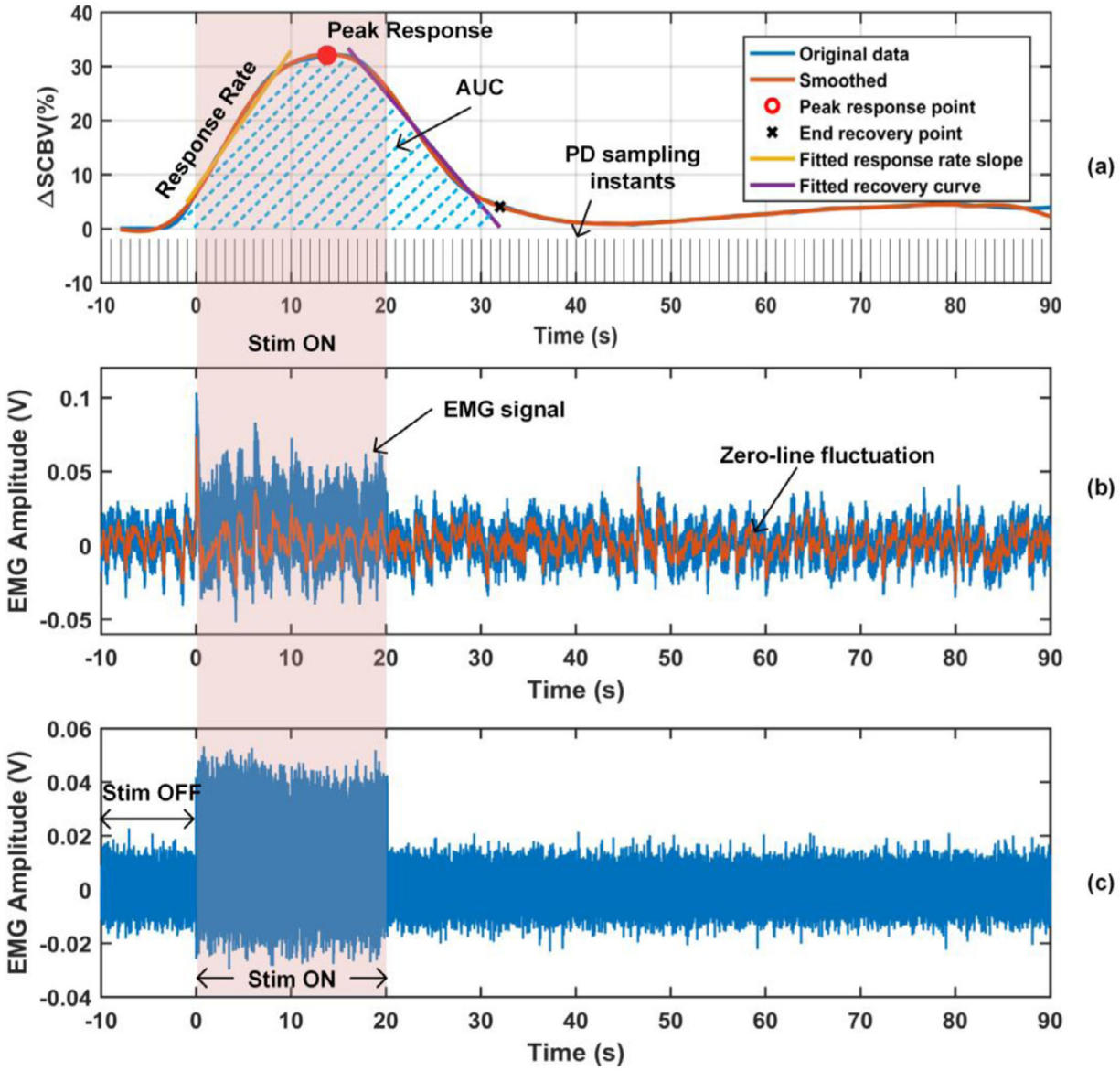

Fig. 2.

ΔSCBV response curve and EMG signal. (a) Parameters including peak response, response rate, and area under the curve (AUC), were measured from a ΔSCBV curve. (b) EMG signal with zero-line fluctuation. (c) EMG signal with the zero-line fluctuation removed.

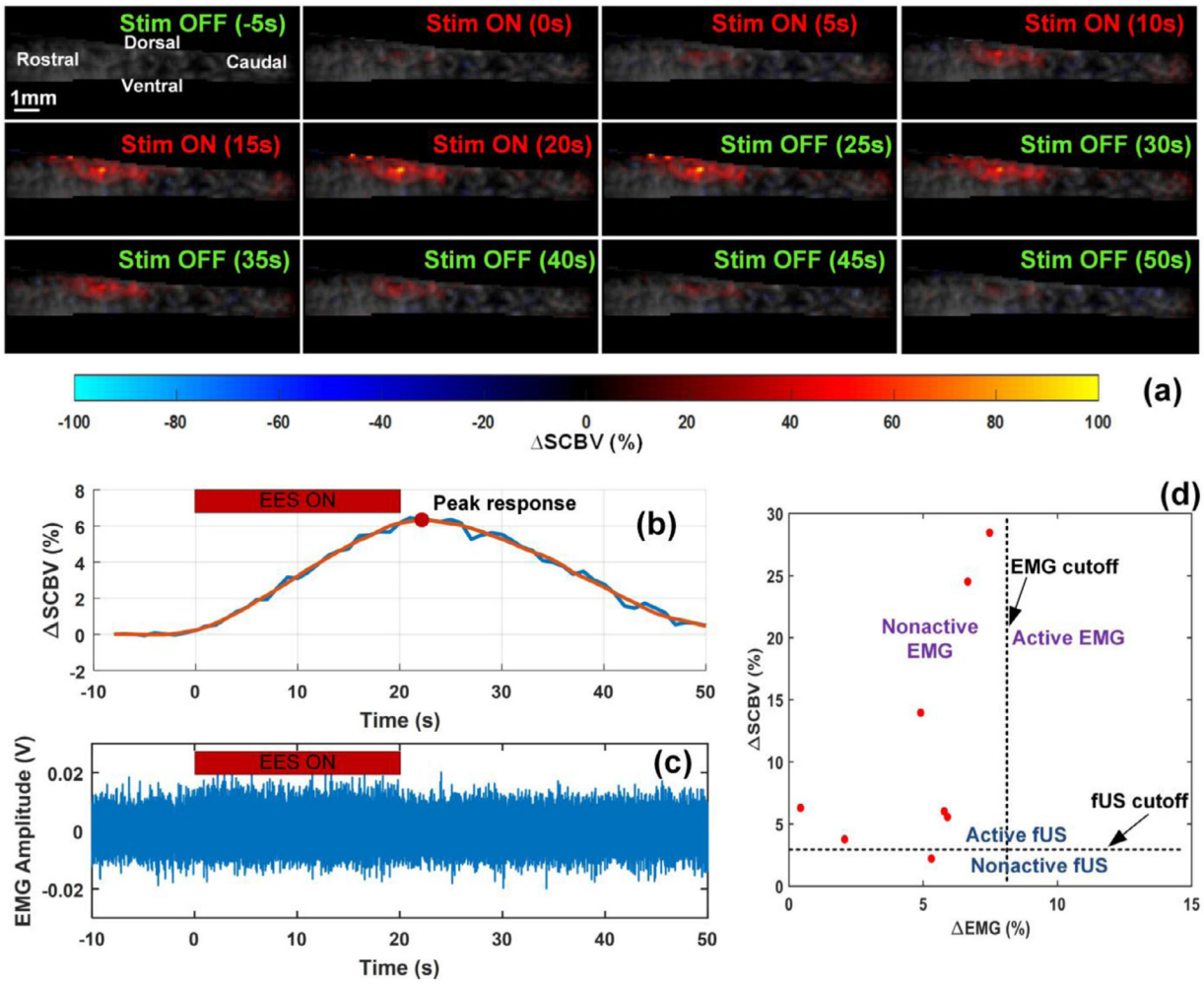

Fig. 3.

fUS is a sensitive technique in monitoring the hemodynamics response of the spinal cord even during subthreshold SCS intensities (i.e. silent EMG). (a) Temporal spinal cord blood volume change (ΔSCBV) color coded on the Power Doppler (PD) images at several point times. A movie is available in the Supplemental video 1. (b) and (c) are ΔSCBV curve and ΔEMG signal for a test with sub-threshold SCS and silent EMG. (d) ΔSCBV peak response vs ΔEMG for the 8 tests with silent EMG signals.

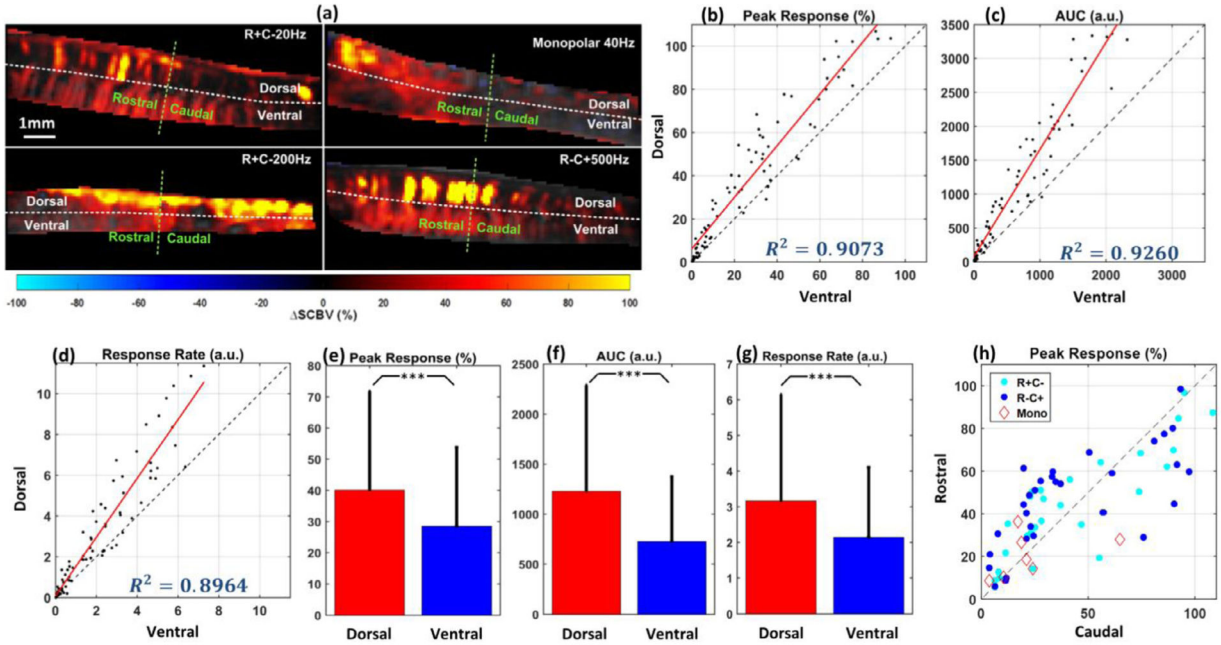

Fig. 4.

Spinal cord hemodynamics response due to SCS is spatially dependent. (a) Representative examples of hemodynamics response images with different SCS parameters and electrode configurations. The four fUS images were collected from supra-threshold intensities, different stimulation frequencies (20 Hz, 40 Hz, 200 Hz and 500 Hz) and electrode configurations (monopolar, bipolar $R+C-$, and bipolar R−$C+$). Ultrasound FOV is divided in dorsal and ventral regions by the white dashed line, and to the rostral and caudal regions with the green dashed line. (b) Peak response of blood volume change in dorsal region vs ventral region (test number, $n = 78$). (c) Total blood volume change over the time (Area under the curve, AUC) for dorsal and ventral regions (test number, $n = 78$). (d) Response rate for dorsal and ventral regions (test number, $n = 78$). (e)–(g) Bar plots of the peak response, AUC and response rate for dorsal and ventral regions. Hemodynamics of the dorsal region of the spinal cord responded significantly higher and quicker to SCS compared to ventral regions, regardless of the stimulation parameter and configuration. (h) Peak response for rostral and caudal regions (test number, $n = 78$). No significant difference between rostral and caudal region was found for either configuration of electrodes. Each data point in (b)–(d) and (h) represents the peak blood volume change in dorsal/ventral or rostral/caudal regions from the same rat with the same stimulation parameter and configuration. Results in (b)–(h) include monopolar and bipolar electrode configurations. For monopolar configuration, SCS intensity includes sub-threshold and supra-threshold and frequency includes 20 Hz and 40 Hz; For bipolar configuration ($R+C-$ and R−$C+$), SCS intensity includes sub-threshold and supra-threshold and SCS frequency includes 20 Hz, 40 Hz, 200 Hz and 500 Hz. ***$p < 0.001$.

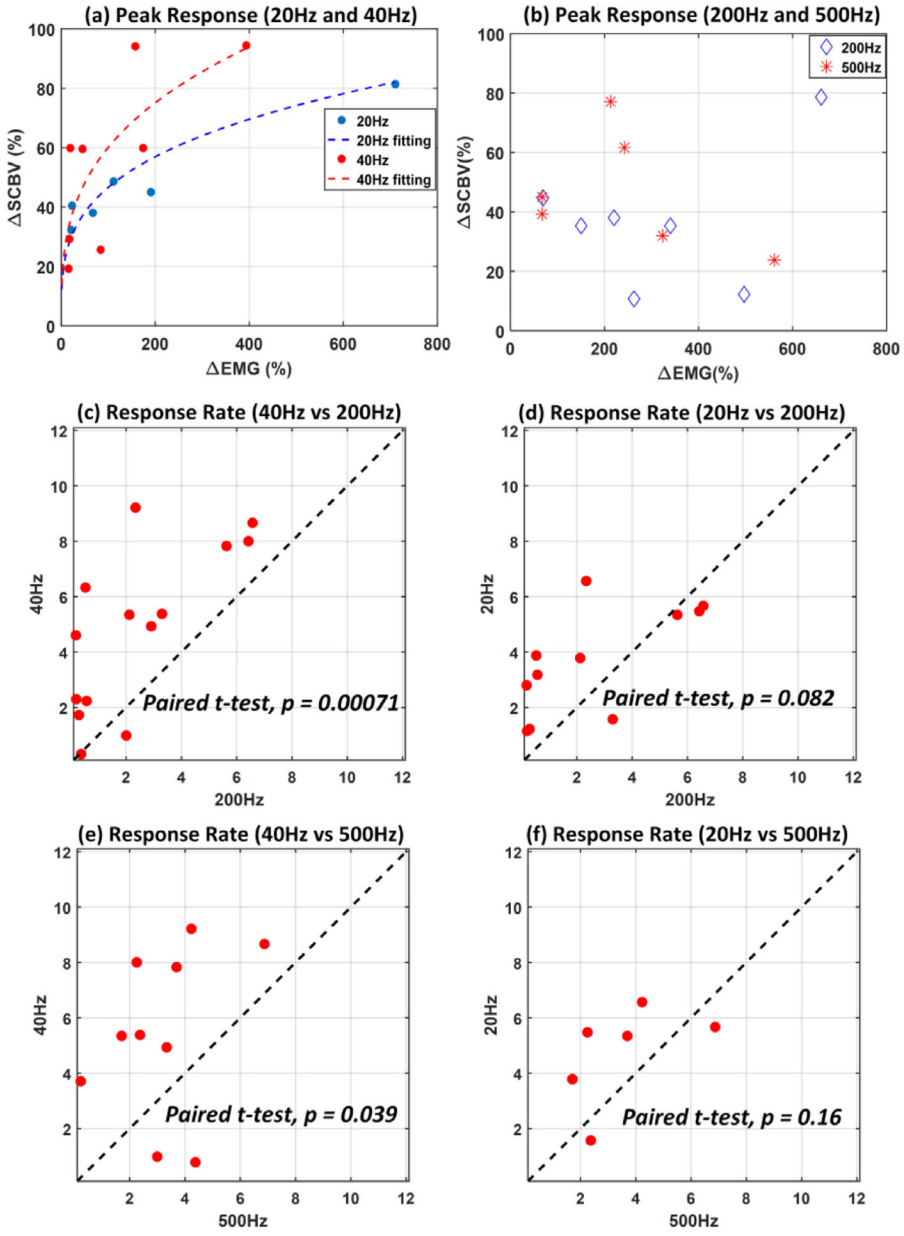

Fig. 5.

SCS produce frequency dependent hemodynamics response within spinal cord. (a) Increase in the hemodynamics response was observed with stimulation frequencies of 20 and 40 Hz (test number, $n = 14$), (b) but not with higher stimulation frequencies of 200 and 500 Hz (test number, $n = 13$). Data presented in (a) and (b) are with electrode configurations including bipolar $R+ C-$ and bipolar R−$C+$, and supra-threshold intensity. (c)–(f) Response rate of the spinal cord to low (20 Hz and 40 Hz) and high (200 Hz and 500 Hz) stimulation frequencies chosen based on our previous findings (I. Lavrov et al., 2008; I. Lavrov et al., 2008; I. Lavrov et al., 2015; I. Lavrov et al., 2015; Gad et al., 2013; Shah and Lavrov, 2017) (test number, $n = 14$ for (c), $n = 11$ for (d), $n = 10$ for (e), and $n = 6$ for (f)). Each dot represents the response rate measured from the two frequencies but the same rat and the

same electrode configuration. Data presented in (c)-(f) are with supra-threshold intensity and electrode configuration including bipolar $R+C-$ and bipolar R$-C+$.